Development of a coupled electro-mechanical model of cylindrical cell LR61 batteries with LS-DYNA ®

Abigail Schauer[1], Megan Gober[1], William O'Donoghue[1], Nathan Spulak[1], George Nelson[1]

[1]*The University of Alabama in Huntsville, Huntsville, AL*

Abstract

In-depth characterization of the mechanical and electrical response of an LR61 alkaline battery is performed, for incorporation into a coupled electro-mechanical battery model using LS-DYNA. Tension tests are performed on the outer metal casing to develop a plasticity model, and a Bayesian Model Calibration analysis is performed to determine crushable foam model parameters for the interior anode, cathode, and separator battery components. Electrochemical impedance spectroscopy, distribution of relaxation times, and Kramers-Kronig analysis are used to determine the electrical response of the battery during incremental crush tests. X-ray imaging is also utilized to determine the dimensions of the inner battery components, and to gain insight into the geometric changes to these individual components that occurs during crushing and the corresponding changes to the electrical behavior. This data is used to determine the required order of a Randles circuit necessary to accurately model the electrical behavior. This experimental data is then incorporated into a solid element LS-DYNA model of the battery utilizing the MAT_24 and MAT_63 material models and the EM_RANDLES_SOLID electrical circuit model.

1 Introduction

Lithium-ion batteries are seeing increased use in consumer products like cell phones and laptops, as well as in automotive electric vehicles and in the emerging electric vertical take-off and landing (eVTOL) aircraft sector. This represents a growing safety risk caused by thermal runaway and ignition of batteries after sustaining damage due to mechanical loading from impacts and crash events. Once ignition occurs, lithium battery fires are extremely difficult to fight, release hazardous chemicals into the environment, and can spontaneously reignite days later [1,2,3]. Multiphysics modeling can help to identify design flaws that might otherwise be missed and help create safer designs that limit ignition during crash and impact events. However for such models to be accurate, it is necessary to first experimentally determine parameters relating to the mechanical and electrical response of the batteries and components, and incorporate these observed responses into the model.

Therefore, mechanical and electrical characterization tests are performed on 1.5V cylindrical cell LR61 alkaline batteries, which are the single cell components within 9V batteries. LR61 batteries are chosen due to the less hazardous nature of alkaline batteries compared to lithium-ion batteries, allowing for safer and easier handling when developing the necessary testing, calibration, and analysis protocols for in-depth battery characterization. In addition changes within the internal components (anode slurry, cathode, and current collector) are more readily observable within single cell batteries, particularly when x-ray imaging is used due to the limited amount of material that the x-rays need to travel through.

Mechanical testing is performed on the outer metal casing to directly determine the mechanical response, and Bayesian Model Calibration is then performed to develop a mechanical model of the internal anode, cathode, and separator components. Electrical characterization is performed on an undamaged pristine battery, as well as during incremental crush testing to evaluate how the battery electrical behavior changes as the battery is deformed. A finite element model of the

LR61 battery is constructed in LS-DYNA, and the measured mechanical and electrical responses are incorporated in order to develop a combined electro-mechanical multiphysics battery model.

2 Mechanical Characterization

The LR61 battery is composed of a cold-drawn steel casing containing a graphite cathode, paper separator and anode slurry with a steel nail in that goes roughly halfway through the central axis. The outer dimensions are 42.5 mm long and 7.8 mm in diameter.

X-ray imaging of the LR61 batteries is conducted using a Hamamatsu 150kV microfocus X-ray source, a Varex PaxScan 2520DX flat panel detector, and efX-DR acquisition software by North Star Industries. An x-ray image of an undamaged pristine LR61 battery is shown in Figure 1(a), with a pixel size of 53.5 µm. The analysis of the intensity and deflection points of the grayscale values in the image is used to determine the dimensions of the internal components of the battery as shown in Figure 1(b). The cathode thickness is determined to be 1.34 mm, the anode slurry is determined to have a radius of 2.28 mm, and the separator has a thickness of 0.32 mm.

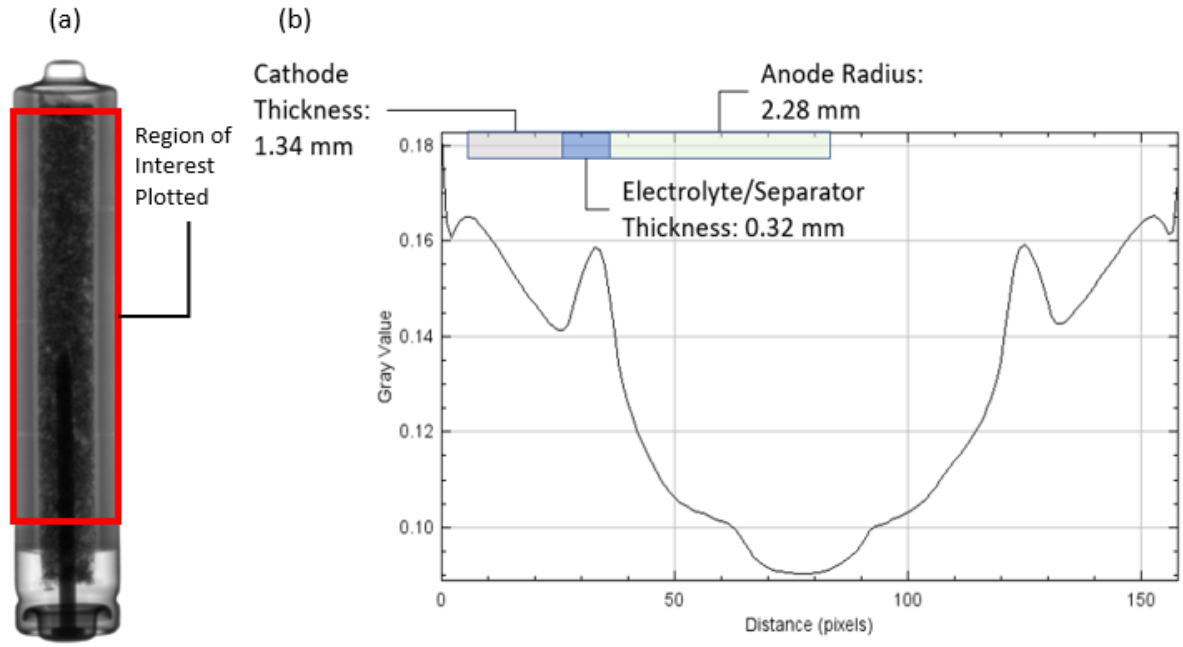

Fig. 1: (a) x-ray image of LR61 battery with region of interest indicated, and (b) grayscale values from region of interest used to determine internal anode, cathode, and electrolyte/separator dimensions

Tension testing is performed on the outer metal casing of the LR61 battery after removing the internal battery components, in order to develop a plasticity model for implementation in LS-DYNA. A dogbone tension profile is milled into the cylindrical shell casing [4], and pipe fittings are used to grip the end sections to prevent damage to the thin shell casing. The milled dogbone specimen is shown in Figure 2(a), and has a gauge length of 10.65 mm, gauge width of 3 mm, and thickness of 0.21 mm. Quasi-static tension tests are performed on a hydraulic load frame, and images are taken during the test for use with digital image correlation (DIC). The engineering stress (σ_E) is determined from the measured force and the initial specimen cross-sectional area, and the engineering strain (ε_E) is measured via a virtual DIC inspect extensometer. The true stress and true strain values are then determined as $\varepsilon_T = \ln(1 + \varepsilon_E)$ and $\sigma_T = \sigma_E(1 + \varepsilon_E) = \sigma_E e^{\varepsilon_T}$. In addition, the local DIC Hencky strain at the fracture location is

measured and taken to be a value of true strain, and this DIC Hencky true strain is used to re-calculate the true stress. The stress vs. strain response is shown in Figure 2(b).

The material was determined to have a Young's modulus of 200 GPa, yield stress of 500 MPa, ultimate stress of 645 MPa, and percent elongation of 7%. The post-yield portion of the DIC Hencky true stress vs. true strain curve is used as the plasticity model for a MAT_24 material model of the metal casing material [5]. The MAT_24 model is validated by performing finite element analysis (FEA) simulations of the tension test, as shown in Figure 3. There is good agreement between the simulated and experimentally measured force vs. displacement response.

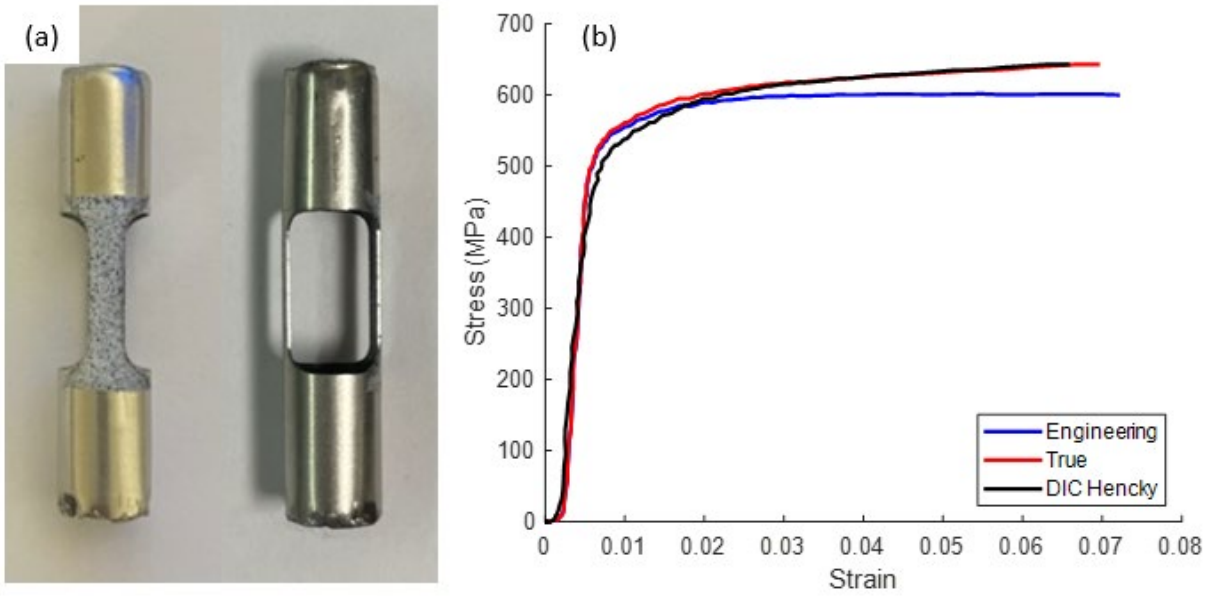

Fig. 2: (a) cylindrical battery casing tension test specimen with milled dogbone profile, and (b) stress vs. strain response of metal casing from uniaxial tension test.

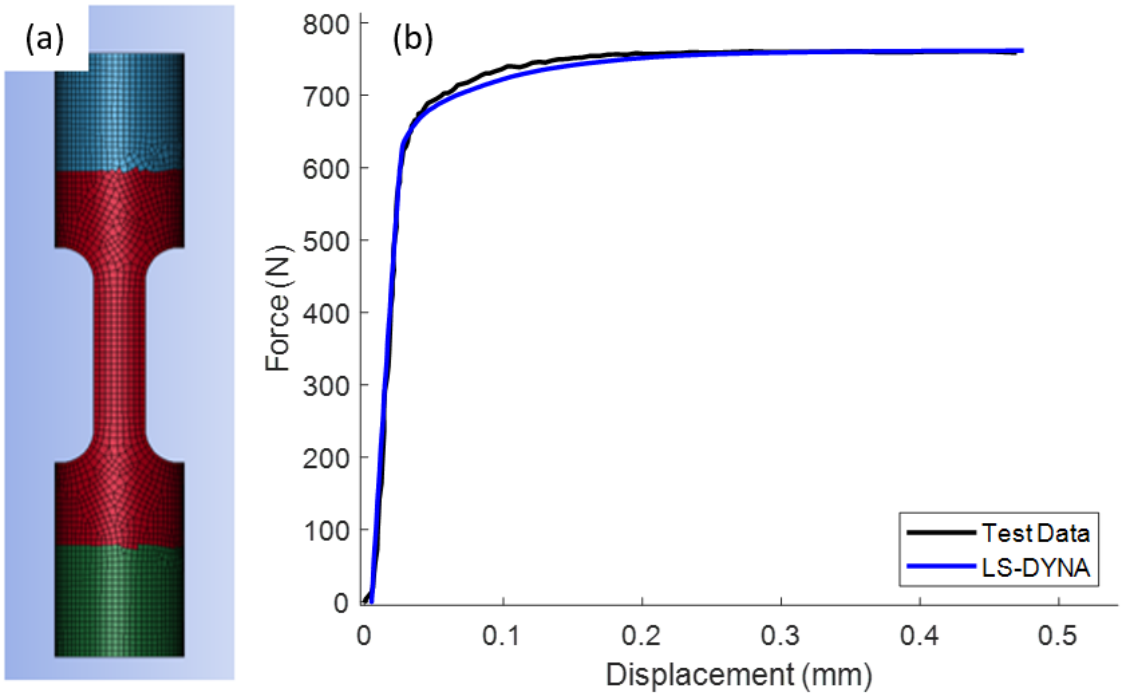

Fig. 3: (a) LS-DYNA model of cylindrical battery shell tension test specimen, and (b) comparison of simulated vs. experimentally measured force vs. displacement response.

The combined mechanical response of the internal anode, cathode, and separator components is modeled as a crushable foam material for use with a MAT_63 material model. Crushable foam was chosen because of its ability to reflect the compacting behaviors of the battery components. Calibration is done by simulating crush tests of the full LR61 battery [6]. The metal battery casing material is modeled using the plasticity curve derived from the tension tests, and the crushable foam model parameters are calibrated to achieve the best fit to the measured force and displacement observed during the full battery crush tests.

The calibration process follows the Bayesian Model Calibration (BMC) procedure outlined by Higdon et al. (2008). This process involves evaluating the FEA simulation at a variety of points in the parameter space, using those results to train a Gaussian Process Model (GPM) to emulate the simulation, and running Markov Chain Monte Carlo (MCMC) to sample from the posterior distribution of the model parameters. The GPM emulators are used to evaluate the response of the model parameters in each MCMC draw in lieu of running the full FEA simulation [6,7].

This approach is applied to calibrate the crushable foam material model parameters, including the ratio of the uniaxial yield stress to hydrostatic yield stress (k), the plastic Poisson's ratio (ν_{pl}), and a coefficient used in an exponential function to define the relationship between the uniaxial yield stress and plastic strain (α) [5]. A Johnson-Cook based damage model is also incorporated and the damage parameters determined for the equivalent plastic strain at which damage begins ($\bar{\varepsilon}_D^{pl}$) and the subsequent plastic displacement until element failure ($\bar{u}_f^{pl}$) [8]. The FEA simulations are run at 120 different locations in the 5th dimensional parameter space using the software package Dakota, and each simulated force-displacement response of the battery is recorded. Features of the experimental and simulated force-displacement curves are used as extracted figures of merit to judge the closeness of each simulated curve to the observed result, and then fed into the SEPIA Python package to run the BMC process [6,9,10]. The resulting posterior distribution for the parameters is shown in Figure 4.

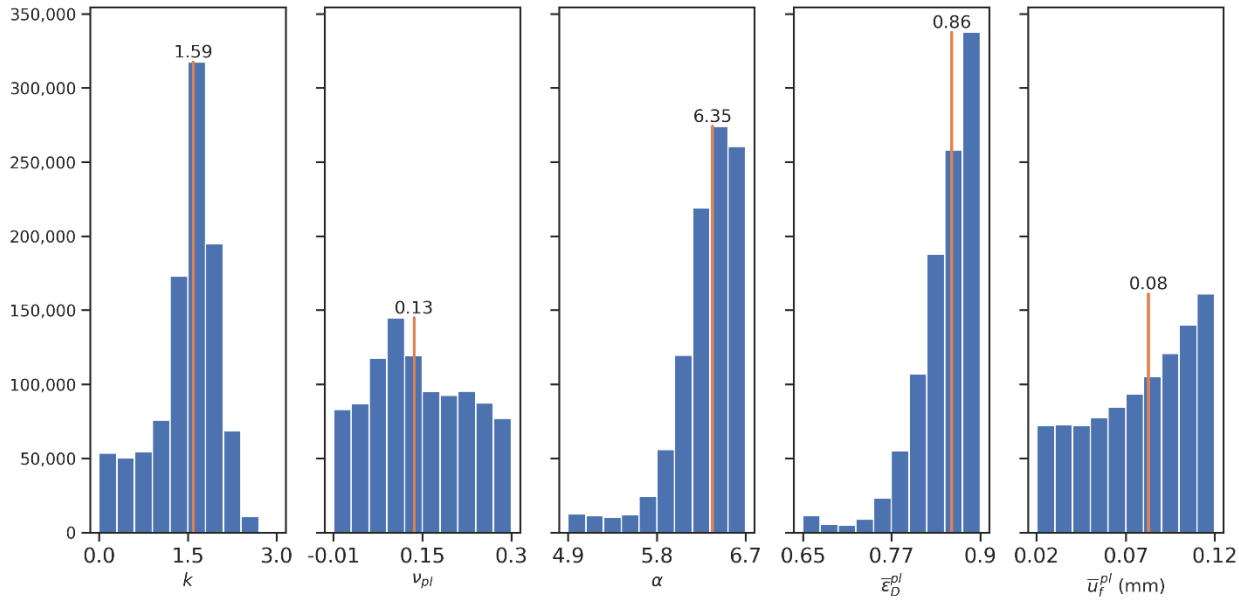

Fig. 4: Posterior distribution of the crushable foam model parameters after 1,000,000 MCMC draws, with the median value shown by the vertical orange lines.

The variable k has a well-defined cluster around 1.59 with lower values more favored than higher values. The plastic Poisson's ratio is less constrained, but with a slight preference for 0.13. The three remaining parameters favor higher values, though $\bar{u}_f^{pl}$ has a higher uncertainty

based on its wide deviation. The ultimate values are determined to be $\alpha = 6.35$, $\bar{\varepsilon}_D^{pl} = 0.86$, and $\bar{u}_f^{pl} = 0.08$ mm.

3 Electrical Characterization

In addition to characterizing the mechanical behavior of the metal casing and internal anode/cathode/separator components of the battery, the electrical response is characterized using the testing methodology developed by Flannagin et al. (2023) to couple electrochemical impedance spectroscopy (EIS) with distribution of relaxation times (DRT) analysis during mechanical loading [11]. Analysis is performed while the LR61 batteries are incrementally crushed in 0.254 mm increments using a Roemheld NC125 Hydro-Mechanical compression vise. X-ray imaging is performed and impedance spectra are gathered at each incremental crushing step.

During external loading, the voltage of the battery changes in response to the applied load. Due to this, EIS scans were conducted at the existing voltage of the battery, using a method commonly known as potentiostatic electrochemical impedance spectroscopy (PEIS), where the sample is held at a fixed potential around the open-circuit voltage. PEIS measurements were taken at each 0.254 mm displacement increments at a frequency range of 3 Hz-100 kHz with 6 points per decade and 6 points averaged per frequency.

The predominant method of analyzing EIS is through the use of equivalent circuit models (ECMs). ECMs allow for the tracking of impedance changes occurring within the cell by correlating them to specific circuit parameters. However it is possible to have multiple circuits that statistically fit the collected data or multiple processes occurring in a similar frequency range. This non-unique nature of ECMs brings challenges to accurately analyzing collected EIS results. To overcome this limitation, DRT has been developed and employed due to its ability to analyze effects even in regions of overlapping frequency [12,13,14,15,16]. Relaxation time is known as the time required for a variable of the system to reach a steady state condition. Such times are characterized by time constants. Since battery systems have multiple complex electrochemical processes, they correspond to a distribution of time constants instead of one single relaxation time constant [12]. DRT analysis converts the impedance spectrum data obtained by EIS from frequency domain to time domain by taking the Fourier transform of the spectrum. In this process the varied time constants of an electrochemical system can be readily visualized.

The x-ray images, EIS, and DRT analysis results from an incremental crush test are shown in Figure 5. The x-ray images in Figure 5(a) show that the pristine battery (0 mm displacement) has observable gaps in the interior anode slurry, likely due to variation within manufacturing. As the battery is compressed, the gap is filled in with anode slurry. The DRT response in Figure 5(b) shows an increase in contact resistances with a respective decrease in charge transfer resistance as displacement is increased. The increase in contact resistances is likely due to connectors becoming compressed, as visible in Figure 5(a). The decrease in charge transfer resistance is likely due to the movement of the anode slurry within the battery, which can introduce new active regions for ion flow, as well as the observable gaps in the anode slurry being filled.

A Kramers-Kronig analysis utilizing the open-source Lin-KK Tool software provided by the Institute for Applied Materials is used to determine whether the gathered EIS data has been influenced by bias errors, such as those caused by instrumental artifacts or time-dependent phenomena [17,18,19]. The Kramers-Kronig relations are integral equations that constrain the real and imaginary components of complex quantities for systems such that the system is stable. This means that perturbations to the system do not grow, that the system responds linearly to a

perturbation, and that the system must be causal such that a response to a perturbation cannot come before the perturbation itself [20].

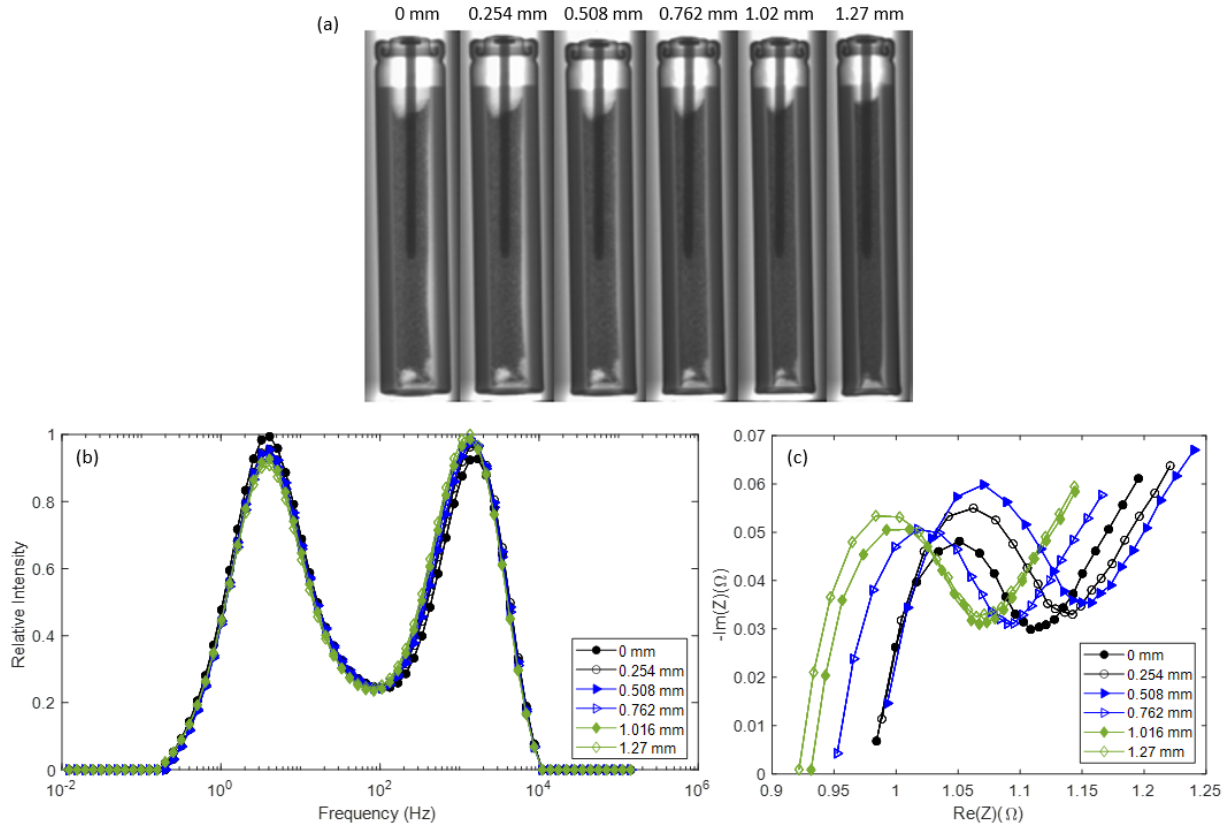

Fig. 5: (a) x-ray images, (b) DRT response, and (c) EIS response of LR61 battery during incremental crush test

The differences between theoretical and experimental impedance values from the Kramers-Kronig analysis is commonly known as the residual [18]. It is desired to have residuals below 1% in order to use the experimental data for further analysis and the extraction of physical constants [21,22]. In addition to determining the quality of data collected, Kramers-Kronig analysis provides useful information regarding the number of Randles circuit elements within a series needed for a proper fit to the experimental EIS results.

Randles circuit ECMs can be implemented within LS-DYNA, utilizing the EM_RANDLES cards. These allow for the direct user input of resistance and capacitance values for up to a 3rd order Randles circuit. If additional complexity is needed, it must be implemented through a user defined function option [5, 23]. Figure 6 shows the results from a Kramers-Kronig analysis for a pristine LR61 sample, comparing the residual fit when a 3rd order Randles circuit and a 14th order Randles circuit are used to model the battery. The residual error is clearly significantly lower with a 14th order Randles circuit compared to a 3rd order one when attempting to fit to the experimental data. The 14th order Randles circuit is well below the 1% residual magnitude required for an acceptable fit, while the 3rd order Randles circuit is barely below 1% and therefore provides a fit that is barely acceptable and borderline unusable.

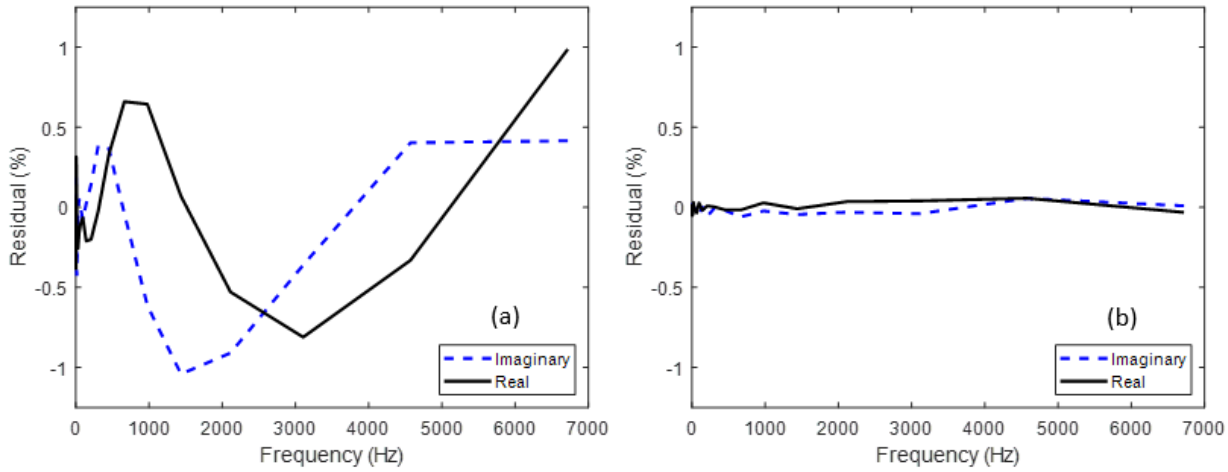

Fig. 6: Kramers-Kronig residual comparison of a pristine LR61 battery using a fit of (a) 3rd order Randles circuit and (b) 14th order Randles circuit.

4 Combined Electro-Mechanical Modeling with LS-DYNA

The mechanical and electrical characterization data is combined in a coupled multiphysics LS-DYNA model of an LR61 battery. The LR61 battery model implemented with LS-DYNA is shown in Figure 7. The battery is meshed with solid elements with an average size of 0.2 mm, while maintaining 67 nodes around the circumference of each layer for the electrical modeling. The metal shell is modeled with the MAT_24 piecewise elastic-plastic material model, using the material properties determined through tension testing. The cathode, separator, and anode materials are modeled with the MAT_63 crushable foam model, using the properties determined via the Bayesian Model Calibration procedure. The central metal nail is modeled using MAT_20 as a rigid material for simplicity.

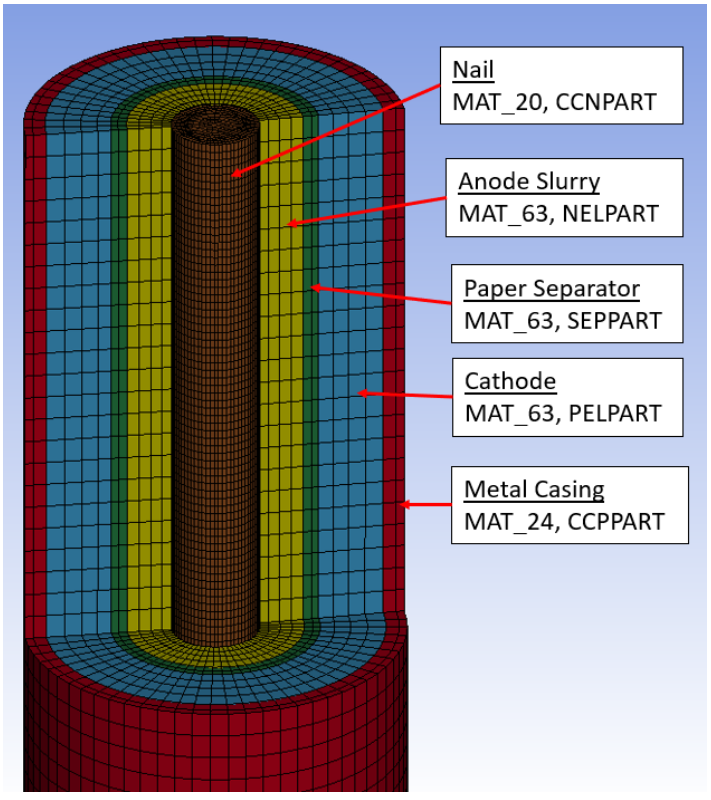

Fig. 7: Coupled electro-mechanical model of LR61 battery implemented within LS-DYNA.

The electrical response is incorporated by defining the individual battery components as different Randles circuit elements, corresponding to their electrical circuit roles within the actual LR61 battery. This is implemented through the use of the EM_RANDLES_SOLID card for use with solid elements. The central nail is defined as the negative current collector (CCNPART), the anode slurry is defined as the negative electrode (NELPART), the paper separator is defined as the separator (SEPPART), the graphite cathode is defined as the positive electrode (PELPART), and the outer metal casing is defined as the positive current collector (CCPPART).

5 Conclusion

The mechanical behavior of an LR61 cylindrical cell battery is determined via a combination of direct testing and inverse model calibration. Tension testing of the outer metal shell is used to develop a MAT_24 piecewise elastic-plastic model, while Bayesian Model Calibration is used to determine the parameters for a MAT_63 crushable foam model for the interior anode, cathode, and separator components. These material models are validated by comparing simulated tension tests and full battery crush tests using these models to the experimentally measured values. In particular, the methodology developed to indirectly determine the mechanical response of the interior battery components through Bayesian Model Calibration is highly desirable, since it is difficult to directly test these interior components due to their fragile and hazardous nature.

The electrical behavior of the battery is investigated using a combined EIS and DRT analysis, in both the undamaged condition and while the battery is undergoing incremental crush testing, so that the changes to battery electrical behavior as it is damaged can be determined. Kramers-Kronig analysis indicates that the use of a 3rd order Randles circuit, as is available within the EM_RANDLES option in LS-DYNA, is insufficient to accurately capture the response of an LR61 battery. A more complex 14th order Randles circuit significantly reduces the residual error, and in order to implement this within LS-DYNA the user defined function option must be used.

An LS-DYNA model of the LR61 battery is constructed containing all the critical battery components. The mechanical and electrical behavior determined via the experimental testing is implemented through the use of MAT_24 and MAT_63 mechanical models, and EM_RANDLES_SOLID option for electrical modeling.

This information can be utilized to more accurately model the battery electrical response during real-world damage and crash events. Future work involves validating the coupled electro-mechanical LS-DYNA model through simulations of LR61 crush tests and comparison of the simulated force, displacement, and voltage response during to the experimentally measured values. Additional future work involves adapting this testing and analysis protocol to lithium-ion batteries, expanding the models of single cell battery behavior to multi-cell battery packs, and incorporating high rate testing and model validation in order to more accurately assess battery safety during dynamic vehicle crash events.

6 References

[1] Duh, Y. S., Lin, K. H., & Kao, C. S. (2018). Experimental investigation and visualization on thermal runaway of hard prismatic lithium-ion batteries used in smart phones. *Journal of thermal analysis and calorimetry*, *132*, 1677-1692.

[2] Victor Chombo, P., Laoonual, Y., & Wongwises, S. (2021). Lessons from the electric vehicle crashworthiness leading to battery fire. *Energies*, *14*(16), 4802.

[3] Barrera, T. P., Bond, J. R., Bradley, M., Gitzendanner, R., Darcy, E. C., Armstrong, M., & Wang, C. Y. (2022). Next-generation aviation li-ion battery technologies—enabling electrified aircraft. *The Electrochemical Society Interface*, *31*(3), 69.
[4] Zhang, X., & Wierzbicki, T. (2015). Characterization of plasticity and fracture of shell casing of lithium-ion cylindrical battery. *Journal of Power Sources*, *280*, 47-56.
[5] LS-DYNA® KEYWORD USER'S MANUAL. (2021). Livermore Software Technology (LST), an Ansys Company.
[6] O'Donoghue, W. (2023). *Bayesian Model Calibration of a Mechanical Finite Element Model of an LR61 Alkaline Battery*. The University of Alabama in Huntsville.
[7] Higdon, D., Gattiker, J., Williams, B., & Rightley, M. (2008). Computer model calibration using high-dimensional output. *Journal of the American Statistical Association*, *103*(482), 570-583.
[8] ABAQUS Theory Manual. (2018). Dassault Systèmes Simulia Corp,, Providence, RI.
[9] Adams, B. M., Bohnhoff, W. J., Dalbey, K. R., Ebeida, M. S., Eddy, J. P., Eldred, M. S., ... & Winokur, J. G. (2020). *Dakota, a multilevel parallel object-oriented framework for design optimization, parameter estimation, uncertainty quantification, and sensitivity analysis: version 6.13 user's manual* (No. SAND2020-12495). Sandia National Lab.(SNL-NM), Albuquerque, NM (United States).
[10] Gattiker, J., Klein, N., Hutchings, G., & Lawrence, E. (2020). lanl/sepia: v1.1. https://doi.org/10.5281/zenodo.4048801
[11] Flannagin, M., Barnes, B., O'Donoghue, W., Mayeur, J., Hazeli, K., & Nelson, G. J. (2023). Electrochemical Response of Alkaline Batteries Subject to Quasi-Static and Dynamic Loading. *Journal of the Electrochemical Society*, *170*(1), 010521.
[12] Chen, X., Li, L., Liu, M., Huang, T., & Yu, A. (2021). Detection of lithium plating in lithium-ion batteries by distribution of relaxation times. *Journal of Power Sources*, *496*, 229867.
[13] Sabet, P. S., & Sauer, D. U. (2019). Separation of predominant processes in electrochemical impedance spectra of lithium-ion batteries with nickel-manganese-cobalt cathodes. *Journal of Power Sources*, *425*, 121-129.
[14] Manikandan, B., Ramar, V., Yap, C., & Balaya, P. (2017). Investigation of physicochemical processes in lithium-ion batteries by deconvolution of electrochemical impedance spectra. *Journal of Power Sources*, *361*, 300-309.
[15] Danzer, M. A. (2019). Generalized distribution of relaxation times analysis for the characterization of impedance spectra. *Batteries*, *5*(3), 53.
[16] Hust, F., Witzenhausen, H., & Sauer, D. U. (2013, June). Distribution of relaxation times for lithium-ion batteries. In *Proceedings of the 9th International Symposium on Electrochemical Impedance Spectroscopy, Okinawa, Japan* (pp. 17-20).
[17] Boukamp, B. A. (1995). A linear Kronig-Kramers transform test for immittance data validation. *Journal of the electrochemical society*, *142*(6), 1885.
[18] Schönleber, M., Klotz, D., & Ivers-Tiffée, E. (2014). A method for improving the robustness of linear Kramers-Kronig validity tests. *Electrochimica Acta*, *131*, 20-27.
[19] Schoenleber, M., & Ivers-Tiffée, E. (2015). Approximability of impedance spectra by RC elements and implications for impedance analysis. *Electrochemistry Communications*, *58*, 15-19.
[20] Orazem, M. E., & Tribollet, B. (2008). Electrochemical impedance spectroscopy. *New Jersey*, *1*(906), 383-389.
[21] Pulido, Y. F., Blanco, C., Anseán, D., García, V. M., Ferrero, F., & Valledor, M. (2017). Determination of suitable parameters for battery analysis by Electrochemical Impedance Spectroscopy. *Measurement*, *106*, 1-11.

[22] Wu, W., Zhuang, Y., Yan, D., Huang, J., Peng, S., Wang, J., ... & Cao, G. (2020). Supercapacitive properties of MnO2 and underlying kinetics by distribution of relaxation time method. *Journal of Power Sources*, *474*, 228667.

[23] Bateau-Meyer, S., L'Eplattenier, P., Deng, J., Zhu, M., Bae, C., & Miller, T. (2018, June). Randles circuit parameters set up for battery simulations in LS-DYNA. In *Proceedings of 15th International LS-DYNA Users Conference*.